American Journal of Engineering Research (AJER)
e-ISSN: 2320-0847 p-ISSN : 2320-0936
Volume-9, Issue-8, pp-99-109
www.ajer.org
Research Paper Open Access

Vibration Analysis and Suppression of Flexible Rotor Systems using a 3-Way Viscoelastic Bearing.

Lawrence Atepor
Department of Mechanical Engineering, Cape Coast Technical University, Box AD 50, Cape Coast, Ghana.

ABSTRACT: *To reduce the severity of vibration emanating from mass unbalance, a 3-way linear viscoelastic end-stops bearing was applied to the flexible rotor system. This paper employs three linear viscoelastic end-stops attached to a linear bearing that acts axially and perpendicularly to improve the performance of the nonlinear flexible rotor system. The model of the rotor-3-way end stops bearing system is established as a modified Jeffcott rotor system. The numerical method of multiple scales is used to solve the equations of motion and the effects of the stiffness and damping ratios of the of the 3-way end stops bearing on the dynamic behavior are discussed. Its stability is then studied using the eigenvalue theory. The instability thresholds of the rotor-3-way end-stops bearing system are obtained varying some parameters of the end-stops bearing. The results show that with dynamic parameters properly designed by using the 3-way viscoelastic end-stops bearing, the amplitude of vibration can be effectively suppressed and the jump can be eliminated. Besides, the 3-way end-stops bearing can change the instability threshold and the instability vibration frequency. It is suggested that the parameters of the 3-way end-stops bearing be selected carefully to suppress the mass unbalance vibration of the rotor system.*

KEYWORDS: *Rotor, Vibration, Suppression, 3-Way viscoelastic end-stops, Stability.*

Date of Submission: 04-08-2020 Date of acceptance: 19-08-2020

I. INTRODUCTION

Vibration in rotating machines is a serious problem, which can lead to failure of machine parts and sometimes to complete shutdown. Control of rotor vibration is very important for safe and stable operation of the machinery Bachschmid et al [1] and Muszynska [2]. Two main methods are mostly employed to control excessive vibration, and they are adjusting of parameters and applying external forces. The mass, stiffness, damping and clearance can be adjusted to suppress the excessive vibration. The dynamic balancing of the rotor is one common method of reducing vibration when the rotor passes the critical speed Zhang et al [3].

Smart materials comprising of Shape Memory Alloys (SMAs) and Piezoelectric Actuators are commonly used to attenuate the rotor vibration by adjusting the stiffness. Atepor [4] presented the Antagonistic SMA/Composite Smart Bearing to control the rotor vibration caused by mass unbalance experimentally. An experimental test machine using a piezoelectric exciter mounted at the end of the shaft of the rotor to adjust the stiffness was used by Atepor [5] to successfully reduce the amplitude of vibration.

Hemmatian and Ohadi [6] used the magnetorheological squeeze film damper to suppress the rotor vibration. In adjusting parameters Queiroz [7] made use of self-adjusted bearing parameters to extend the stability margins for the rotor system in investigating the active fluid-film bearing of the rotor system. In applying external force, Janik et al [8] proposed the use of force generated by electromagnetic exciters to control vibration in the rotor-shaft system.

Viscoelastic materials have long been used as an efficient means of mitigating vibration and noise. They also exhibit the memory effect and their stiffness and damping properties depend on frequency and temperature Rade et al [9]. Viscoelastic materials have been successfully applied in a variety of engineering systems such as industrial equipment, airplanes, automobiles and civil constructions Bachschmid et al [1] and Muszynska [2]. Ribeiro et al [10] presented the viscoelastic supports for the vibration control in rotating machines. The above ideas have lead to the proposed design of a 3-way linear viscoelastic end-stops bearing that acts both axially and perpendicularly on the flexible rotor system to moderate the response of the pre-existing mass unbalance vibration inherent in the rotor. The idea here is to use the 3-way viscoelastic end-stops

bearing to adjust the stiffness of the shaft both axially and laterally and to manipulate some of the parameters such that the inherent and predominant instabilities in the rotor system can be suppressed.

Section "Mathematical Model and Perturbation Analysis" describes the dynamic model of the flexible rotor system with the 3-WESB and the analytical solutions of the developed model equations. Sub-Section "Calculation and Selection of the Spring Constant k_4" describes the method used in selecting the spring used for keeping the 3-WESB setup in constant contact with the rotor shaft end. Section "Nonlinear Dynamic Analysis of the Flexible Rotor System" compares plots obtained from direct numerical integration using NDSolve integrator of the fourth order Runge-Kutta technique and that from the perturbation method of multiple scales. In the sub-section " Effects of 3-WESB Parameters on Resonance Responses" the effects of the 3-WESB parameters on resonance responses compared with that of the rotor system without the 3-WESB is illustrated. Three cases are considered: When $\rho_3 = 0$ in case A, when $\zeta_3 = \text{constant}$ and ρ_3 is varied in case B and when $\rho_3 = \text{constant}$ and ζ_3 is varied in case C. The section " Stability of the Rotor-3-WESB System" compares the stability of the rotor system with and without the 3-WESB. The conclusions are stated in the section "Conclusion".

II. MATHEMATICAL MODEL

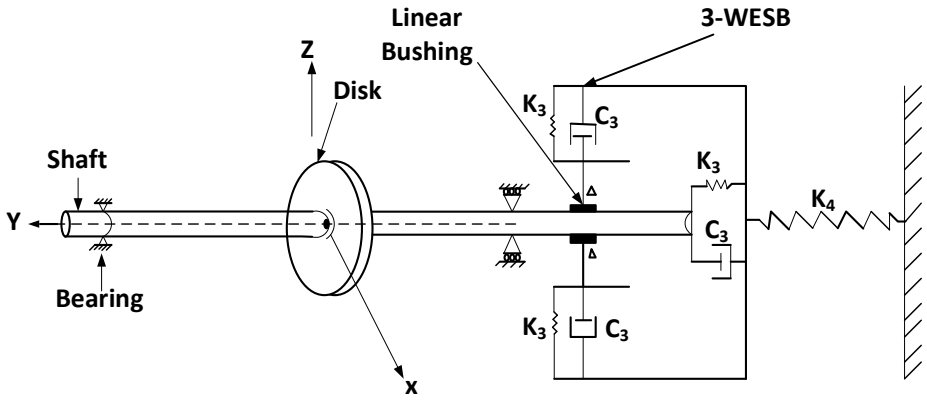

Fig. 1. A Jeffcott Rotor System with a 3-Way Elastomeric End-Stops Bearing

A vibration controller model with a 3-Way elastomeric end-stops bearing (3-WESB) is considered as shown in Fig.1, which can be used to describe a flexible rotor system with the shaft end fitted to an end-stops bearing arrangement. The bearing is made of linear bushings and is for combined linear and rotary motion and it allows high speed with low friction. As attention is focused on the examination of the primary resonance, it is necessary to consider nonlinear characteristics of the system. The end-stops come into action mainly in domain around resonance which is only transient, thus, the linear assumption for the elastomeric end-stops. The equations of motion for the rotor system can be written as

$$\ddot{x} + \hat{c}\dot{x} - \Omega\hat{a}_5\dot{y} + \omega^2 x + \hat{b}x^3 - G(x,\dot{x}) = \Gamma\Omega^2 \sin\Omega t$$

$$\ddot{y} + \hat{c}\dot{y} + \Omega\hat{a}_5\dot{x} + \omega^2 y + by^3 - G(y,\dot{y}) = \Gamma\Omega^2 \cos\Omega t \tag{1}$$

Where, $\hat{a}_5 = \frac{a_5}{m}, \omega^2 = \frac{k}{m}, \hat{b} = \frac{b}{m}, \hat{c} = \frac{c}{m}, \Gamma = \frac{m_u d}{m}$, k –linear stiffness coefficient, c -damping coefficient, x, y -displacements, ω -natural frequency, b -nonlinear cubic stiffness coefficient, Ω -excitation frequency, m -mass of the disk, m_u -mass unbalance situated at a distance d from the geometric centre of the shaft, a_5 -characteristic equation coefficient associated with inertia, ω is the linear undamped natural frequency of the free vibration and

$$G(x,\dot{x}) = \frac{g}{m}(x,\dot{x}) = \omega_3^2 x^2 + \hat{c}_3 x\dot{x} + \omega_4^2 y + 2\omega_3^2 x + 2\hat{c}_3\dot{x}$$

$$G(y,\dot{y}) = \frac{g}{m}(y,\dot{y}) = \omega_3^2 y^2 + \hat{c}_3 y\dot{y} + \omega_4^2 x + 2\omega_3^2 y + 2\hat{c}_3\dot{y} \tag{2}$$

The parameters of the 3-WESB are considered as follows. Picking the mass ratio as $\varepsilon_\varepsilon = 0.01$, since the 3-WESB's mass ratio is limited for the practical consideration. It is known that the mass unbalance induced

vibration frequency is almost equal to the natural frequency of the rotor, for this, the natural frequency of the 3-WESB is taken to be equal to that of the natural frequency of the rotor system.

Where, $\omega_3^2 = \omega^2 = \frac{k_3}{m_3}, \hat{c} = \frac{c}{m}, \zeta = \frac{\hat{c}}{2\omega}, \hat{c}_3 = \frac{c_3}{m}, \zeta_3 = \frac{\hat{c}_3}{2m_3\omega}, \varepsilon_\varepsilon = \frac{m_3}{m} = 0.01, \omega_4^2 = \frac{k_4}{m_3}, \rho_3 = \frac{\omega_3}{\omega}, \rho_4 = \frac{\omega_4}{\omega}, k_3$ – stiffness coefficient of the 3-WESB, m_3 - mass of the 3-WESB, c_3 -damping coefficient of the 3-WESB and k_4 –linear stiffness coefficient of the supporting spring.

2.1 Calculation and selection of the spring constant k_4

As the rotor whirls there will be millimeter level axial contraction of the shaft leaving a gap which will have to be taken up by the 3-WESB. The 3-WESB will have to follow the end of the shaft as it contracts, but because the other end of the 3-WESB has to react against something, a spring is needed to provide sufficient reaction, and to take up the space left as the mass moves upwards. The maximum spring force available is given in equation (3)

$$F_{s\max} = k_4\delta_2 \quad (3)$$

Where, F_{smax} is the maximum spring force, k_4 is the spring constant and δ_2 is the maximum spring compression. Fig. 2(b) shows the shaft having displaced to the left as a consequence of whirl. The spring has extended to fill the gap, Δ, and the remaining spring compression is δ_1 This is a pre-compression and is set up via equation (4) such that it satisfies the need for the minimum spring force (F_{smin}) offered by the spring to equal at least the maximum force which the 3-WESB is capable of $F_{B,}$ meaning

$$F_{s\min} = F_B = k_s\delta_1 \quad (4)$$

Where, δ_1 is the 'preload' pre-compression. As the minimum spring force available must be enough to resist the maximum force generated by the 3-WESB, the 3-WESB then can transmit its force to the shaft, even when the shaft has travelled by its maximum displacement upwards. The free length of the spring is as shown in Fig. 2(c). It can easily be seen that the relationship between the pre-compression δ_1 , the maximum compression δ_2 , and the maximum displacement, Δ ,is given by the equation (5)

$$\delta_1 = \delta_2 - \Delta \quad (5)$$

This means that the maximum spring force can be written as in equation (6)

$$F_{s\max} = k_4\left(\delta_1 + \Delta\right) \quad (6)$$

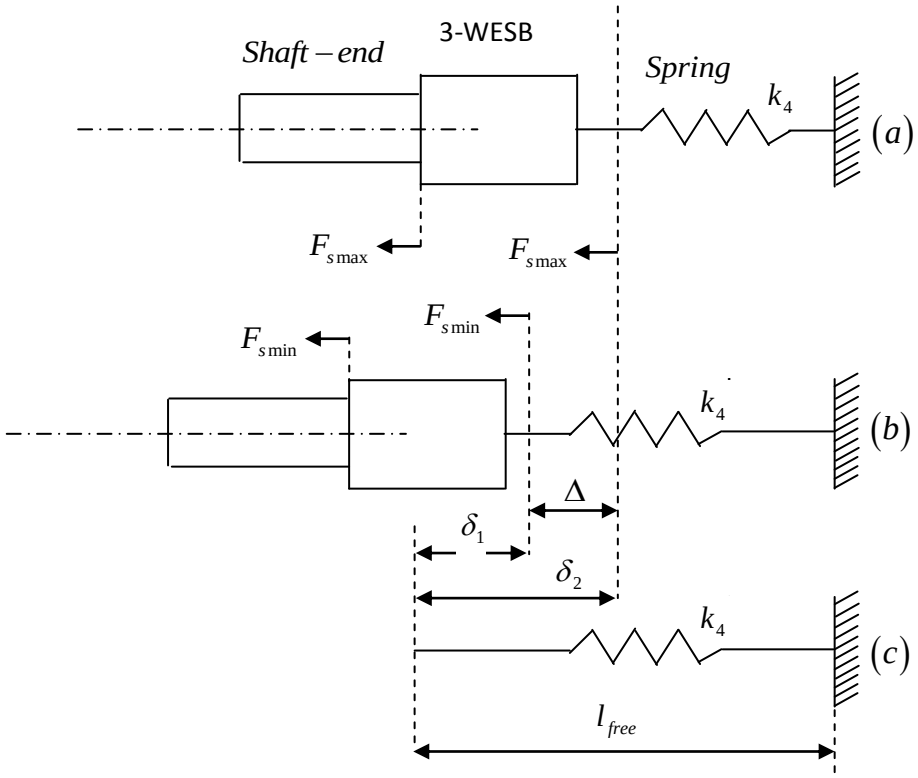

Fig. 2. (a) Shaft-end assembly when rotor is not whirling, (b) Shaft-end assembly when the rotor is whirling at maximum amplitude. (c) Free length of spring.

A spring was chosen based on the maximum required spring force and hence stiffness was obtained. Equation (1) was used to find the force F_B that is actually needed for the system. The NDSolve integrator within Mathematica™ code was employed to solve the differential equation. All other parameters were fixed and the force term F_B value was varied until a parametric plot was obtained as shown in Fig. 3 and the value at which the response is predicted was taken as a threshold value for the force F_B.

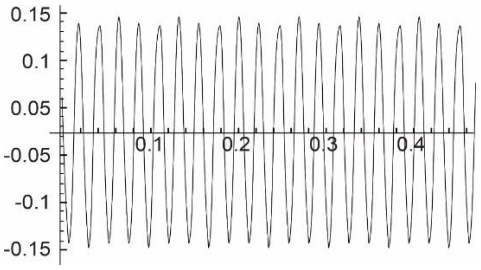

Fig. 3. Parametric Plot

The axial loading relationship $F_B = \frac{AE}{l}\Delta$ is used in finding the maximum displacement Δ, where the parameters for the calculation of spring are as follows: F_B is the 3-WESB force of 332N, $A = \pi r^2$ where r is the radius of the shaft, E is the modulus of elasticity of steel and l is the shaft length of 0.56m.

Therefore

$$\Delta = \frac{Pl}{AE} = 0.018 \tag{7}$$

Now

$$\delta_2 = L_0 - L_n = 25.2mm \tag{8}$$

Giving

$$\delta_1 = \delta_2 - \Delta = 25.182mm \tag{9}$$

Spring constant is

$$k_4 = \frac{F_{S\min}}{\delta_1} = 13184Nm^{-1} \tag{10}$$

Therefore

$$F_{S\max} = k_4\delta_2 = 332.2N \tag{11}$$

III. PERTURBATION ANALYSIS

We nondimensionalise the time scale t and order the equations (1) and (2) by introducing the small parameter ε. Let nondimensional time τ be $\tau = \omega t$, where, ω is normalised to unity, therefore $\tau \cong 1$. Thus equations (1) and (2) can be written as

$$\bar{x}'' + \varepsilon\frac{\bar{c}}{\omega}\bar{x}' - \frac{\Omega}{\omega}\bar{a}_5 y' + \bar{x} + \varepsilon^2\frac{\hat{b}}{\omega^2}\bar{x}^3 - \varepsilon\rho_3^2\bar{x}^2 - \varepsilon\frac{\bar{c}_3}{\omega}\bar{x}\bar{x}' - \varepsilon\rho_4^2\bar{y} - 2\varepsilon\rho_3^2\bar{x} - 2\varepsilon\frac{\bar{c}_3}{\omega}\bar{x}' = \bar{\Gamma}\left(\frac{\Omega}{\omega}\right)^2\sin\left(\frac{\Omega}{\omega}t\right)$$

$$\bar{y}'' + \varepsilon\frac{\bar{c}}{\omega}\bar{y}' + \frac{\Omega}{\omega}\bar{a}_5\bar{x}' + \bar{y} + \varepsilon^2\frac{\hat{b}}{\omega^2}\bar{y}^3 - \varepsilon\rho_3^2\bar{y}^2 - \varepsilon\frac{\bar{c}_3}{\omega}\bar{y}\bar{y}' - \varepsilon\rho_4^2\bar{x} - 2\varepsilon\rho_3^2\bar{y} - 2\varepsilon\frac{\bar{c}_3}{\omega}\bar{y}' = \bar{\Gamma}\left(\frac{\Omega}{\omega}\right)^2\sin\left(\frac{\Omega}{\omega}t\right)$$

(12)

Then, the multiple scales method is used with the following approximate solution Cartmel et al [11] and Nayfeh & Mook [12].

$$\bar{x}(t,\varepsilon) = \bar{x}_{10}(T_0,T_1) + \varepsilon\bar{x}_{11}(T_0,T_1) + O(\varepsilon^2)$$

$$\bar{y}(t,\varepsilon) = \bar{y}_{10}(T_0,T_1) + \varepsilon\bar{y}_{11}(T_0,T_1) + O(\varepsilon^2)$$

(13)

where, $\bar{x}_{10}(T_0,T_1)\ldots\bar{y}_{11}(T_0,T_1)$ are functions of time scales $T_n = \varepsilon^n t$ for $n = 0,1,\ldots$ T_0 is nominally considered as a fast time-scale and T_1 as slower time-scale, such that $T_0 = t$, $T_1 = \varepsilon t$. It follows that the derivatives with respect to t become expansions in terms of the partial derivatives with respect to the T_n according to

$$\frac{d}{dt} = \frac{dT_0}{dt}\frac{\partial}{\partial T_0} + \frac{dT_1}{dt}\frac{\partial}{\partial T_1} + \frac{dT_2}{dt}\frac{\partial}{\partial T_2} = D_0 + \varepsilon D_1 + \varepsilon^2 D_2$$

$$\frac{d^2}{dt^2} = D_0^2 + 2\varepsilon D_0 D_1 + 2\varepsilon^2 D_0 D_2 + \varepsilon^2 D_1^2 \tag{14}$$

Applying Eqs. (13) and (14) to (12) and solving leads to the equation (15) describing the relationship between excitation amplitude Γ, the detuning parameter, $\bar{\sigma}$ and the system's responses. This is a frequency–response equation, which is a measure of deviation from the perfect forced primary resonance condition.

$$\bar{\sigma} = 2 - \frac{\hat{a}_5\Omega}{2\omega} \pm \frac{4}{\Gamma}\left[2\left(4\rho_4^2 a + 8\rho_3^2 a - 4\zeta a + 2\zeta^2 a - \frac{\hat{a}_5^2\Omega^2}{2\omega^2}a - \frac{12\hat{b}}{\omega^2}a^3 - 2\zeta\rho_4^2 a - 4\zeta\rho_3^2 a - 8\varepsilon_\varepsilon\zeta\zeta_3 a\right)^2\right]^{\frac{1}{2}}$$

(15)

IV. NONLINEAR DYNAMIC ANALYSIS OF THE FLEXIBLE ROTOR SYSTEM

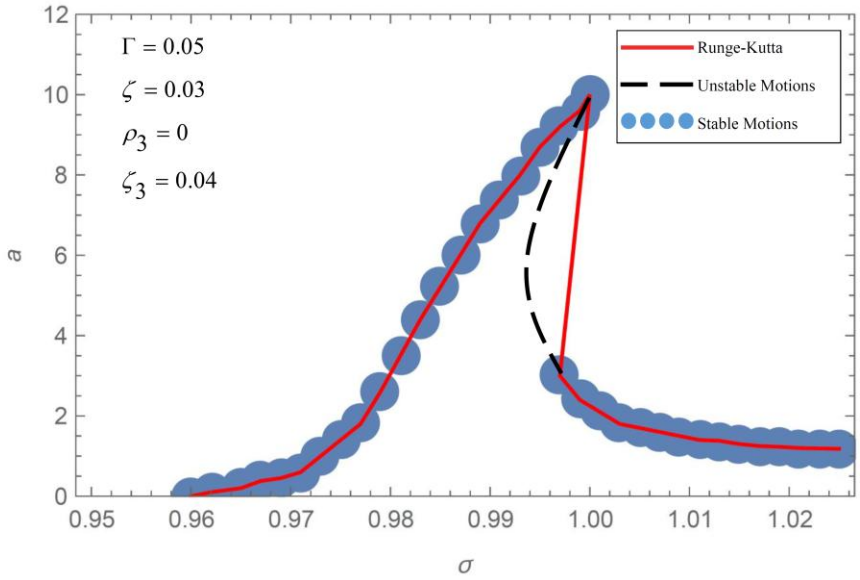

Fig. 4. Comparison between analytical and numerical frequency responses.

As shown in Fig. 4, the frequency response curves of the rotor system are plotted. The multiple scales method results are compared with the numerical results obtained through NDSolve of the fourth order Runge-Kutta technique. It can be observed that the approximate solutions and the numerical solutions are in excellent agreement. The results show evidence of a consistent phenomenon whereby the responses in the first mode show hardening characteristics, jump phenomena and both stable and unstable solutions.

4.1Effects of 3-WESB Parameters on Resonance Responses

In this section, keeping Γ and ζ constant, first mode response curves are obtained for varying the parameters ρ_3, ζ_3 of the 3-way end-stops. In all the diagrams, the dotted lines represent stable motions, while the dashed lines represent the unstable motions. The jump phenomena occur at certain critical points when the frequency is increasing or decreasing.

Case A: $\rho_3 = 0$

As shown in Fig.5, the degree of nonlinearity is not changed when ζ_3 varies. However, varying and increasing the damping ratio ζ_3 of the 3-WESB from 0.04 to 0.07 results in amplitude reduction of frequency responses from 12 to 8 and a shift in frequency from 1 to 0.99. Therefore, activating the 3-WESB has effect on the amplitude of vibration in the first mode of the nonlinear rotor system.

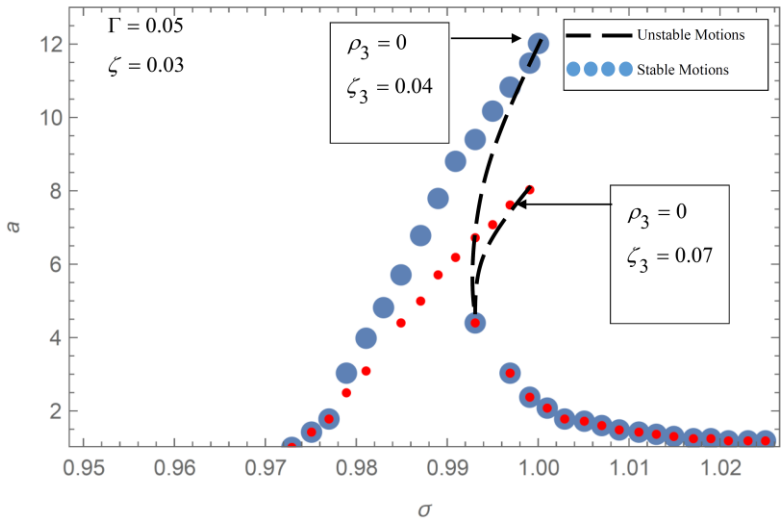

Fig. 5. Frequency-response curves when $\rho_3 = 0$, and ζ_3 is varied.

Case B: $\zeta_3 = \text{Constant}$

In this subsection, the value of the design parameter ζ_3 for the 3-WESB is kept constant and ρ_3 is varied and their effects on the frequency response are examined as shown in Fig. 6. Increasing the ρ_3 from $0 \rightarrow 0.5 \rightarrow 1$ results in higher peak amplitudes ranging from $7 \rightarrow 8 \rightarrow 8.8$ respectively and with the backbones of the curves bending more severely to the right. This shows that the positive stiffness of the 3-WESB brings a more hard nonlinearity to the system. Therefore, a too stiff end-stop when compared to the stiffness of the rotor system can be detrimental to the amplitude suppression being sort, since it rather caused the amplitude level to increase. However, it is able to shift the resonance levels backward and forward, that is from $0.991 \leftarrow 1 \rightarrow 1.015$ respectively.

Case C: $\rho_3 = \text{Constant}$

In this subsection the value of the parameter ρ_3 is kept constant at $\rho_3 = 0.05$ and ζ_3 is varied and their effects on the frequency response are examined as shown in Fig. 7. Increasing the values of ζ_3 from $0.04 \rightarrow 0.07 \rightarrow 0.09$ results in the peak amplitude values decreasing from $10 \rightarrow 8 \rightarrow 6.2$ respectively. This further shows that choosing the correct set of parameters for the 3-WESB can result in reduction of the amplitude and in this particular case by 38% when ζ_3 is deliberately increased from 0.04 to 0.09 which is consistent with results obtained in Atepor (2008).

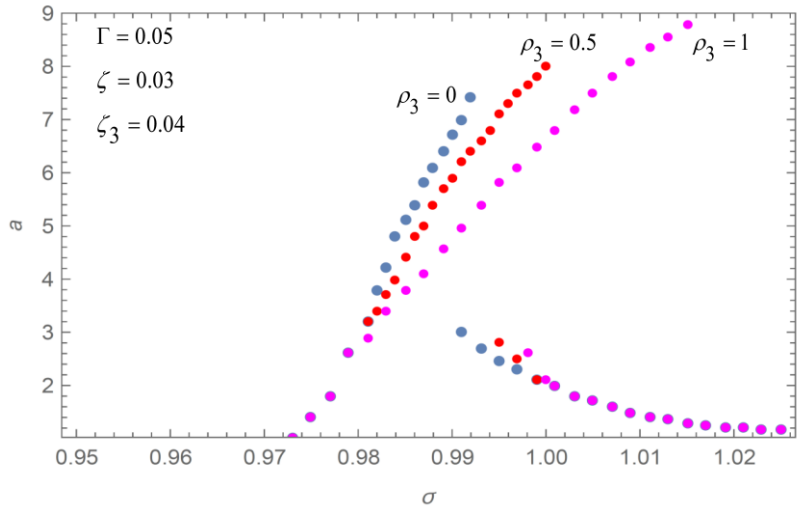

Fig.6 . Frequency-response curves when $\zeta_3 = \text{constant}$ **, and** ρ_3 **is varied.**

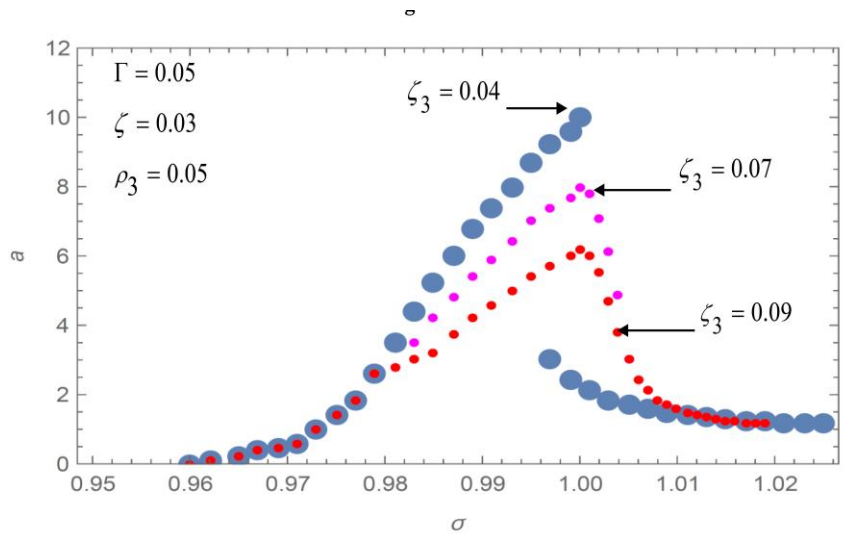

Fig. 7. Frequency-response curves when $\rho_3 = \text{constant}$ **, and** ζ_3 **is varied.**

V. STABILITY OF THE ROTOR-3-WESB SYSTEM

This section derives the natural frequencies of the rotor-3-WESB system. The natural frequency and damping of the 3-WESB can influence the stability threshold of the flexible rotor system therefore the stability region of the flexible rotor system is examined under the influence of the 3-WESB. Taking the nonlinear terms out and equating the mass-unbalance to be zero we have the nonlinear equations of (1) becoming linear and are as stated in equation (16). The equations in (1) are linearized for the stability analysis using the eigenvalue theory.

$$\ddot{x}+\hat{c}\dot{x}-\Omega\hat{a}_5\dot{y}+\omega^2 x-2\omega_3^2 x-2\hat{c}_3\dot{x}-\omega_4^2 y=0$$
$$\ddot{y}+\hat{c}\dot{y}+\Omega\hat{a}_5\dot{x}+\omega^2 y-2\omega_3^2 y-2\hat{c}_3\dot{y}-\omega_4^2 x=0$$

(16)

Let, $x=A_1e^{i\omega_e t}$ and $y=A_2e^{i\omega_e t}$ then we have

$$-A_1\omega_e^2e^{i\omega_e t}+i\hat{c}A_1\omega_e e^{i\omega_e t}-i\Omega\hat{a}_5A_2\omega_e e^{i\omega_e t}+\omega^2A_1e^{i\omega_e t}-2\omega_3^2A_1e^{i\omega_e t}-2i\hat{c}_3A_1\omega_e e^{i\omega_e t}-\omega_4^2A_2e^{i\omega_e t}=0$$
$$-A_2\omega_e^2e^{i\omega_e t}+i\hat{c}A_2\omega_e e^{i\omega_e t}+i\Omega\hat{a}_5A_1\omega_e e^{i\omega_e t}+\omega^2A_2e^{i\omega_e t}-2\omega_3^2A_2e^{i\omega_e t}-2i\hat{c}_3A_2\omega_e e^{i\omega_e t}-\omega_4^2A_1e^{i\omega_e t}=0$$

(17)

Dividing throughout by $e^{i\omega_e t}$ and rearranging leads to

$$\left(i\hat{c}\omega_e-\omega_e^2+\omega^2-2\omega_3^2-i2\hat{c}_3\omega_e\right)A_1-\left(i\hat{a}_5\Omega\omega_e+\omega_4^2\right)A_2=0$$
$$\left(i\hat{a}_5\Omega\omega_e-\omega_4^2\right)A_1+\left(i\hat{c}\omega_e-\omega_e^2+\omega^2-2\omega_3^2-i2\hat{c}_3\omega_e\right)A_2=0$$

(18)

For $A_1\neq 0$ and $A_2\neq 0$

Let the determinant of equations in (18) be zero

$$\begin{vmatrix} i\hat{c}\omega_e-\omega_e^2+\omega^2-2\omega_3^2-i2\hat{c}_3\omega_e & -i\hat{a}_5\Omega\omega_e-\omega_4^2 \\ i\hat{a}_5\Omega\omega_e-\omega_4^2 & i\hat{c}\omega_e-\omega_e^2+\omega^2-2\omega_3^2-i2\hat{c}_3\omega_e \end{vmatrix}$$

(19)

Solving equation (19) leads to

$$\omega_e^4+\left(4\omega_3^2-\hat{c}^2+4\hat{c}\hat{c}_3-2\omega^2-4\hat{c}_3^2-\hat{a}_5^2\Omega^2\right)\omega_e^2+\left(\omega^4-4\omega_3^2\omega^2+4\omega_3^4+\omega_4^4\right)=0$$

(20)

Let $\sigma=\omega_e^2$, then equation (20) becomes

$$\sigma^2+\left(4\omega_3^2-\hat{c}^2+4\hat{c}\hat{c}_3-2\omega^2-4\hat{c}_3^2-\hat{a}_5^2\Omega^2\right)\bar{\sigma}+\left(\omega^4-4\omega_3^2\omega^2+4\omega_3^4+\omega_4^4\right)=0$$

Thus,

$$\sigma=\frac{1}{2}\left[\left(\hat{c}^2-4\hat{c}\hat{c}_3+2\omega^2+4\hat{c}_3^2+\hat{a}_5^2\Omega^2-4\omega_3^2\right)\pm\sqrt{\left(4\omega_3^2-\hat{c}^2+4\hat{c}\hat{c}_3-2\omega^2-4\hat{c}_3^2-\hat{a}_5^2\Omega^2\right)^2-\left(4\omega^4-16\omega_3^2\omega^2+16\omega_3^4+4\omega_4^4\right)}\right]$$

(21)

Becoming,

$$\sigma=1+2\zeta^2-2\rho_3^2-8\varepsilon_\varepsilon\zeta\zeta_3+8\varepsilon_\varepsilon\zeta_3^2+\frac{\hat{a}_5^2\Omega^2}{\omega^2}$$
$$\pm\left[4\rho_3^2-4\rho_3^4-\rho_4^4-1+\frac{1}{4}\left(4\rho_3^2-4\zeta^2+8\varepsilon_\varepsilon\zeta\zeta_3-1-8\varepsilon_\varepsilon^2\zeta_3^2-\frac{\hat{a}_5^2\Omega^2}{\omega^2}\right)^2\right]^{\frac{1}{2}}$$

(22)

The complex eigenvalues are obtained from equation (22). The system's response is said to be stable when the eigenvalue is negative and real. With a real but zero value the response is said to be at the threshold of stability. The response becomes unstable when the eigenvalue is positive and real.

The instability threshold plots of the flexible rotor system with the 3-WESB are presented in Figs. 8 to12. The red lines represent the instability threshold of the rotor system without the 3-WESB and the blue lines represent the instability threshold of the rotor system with the 3-WESB. Figs. 8 to 12 show the effect of the natural frequency of the 3-WESB on the stability of the system. As σ increases, the instability threshold of the system with the 3-WESB is at first smaller, then bigger and again becomes smaller than the system without the 3-WESB. In Fig. 8, at $\zeta_3 = 0.01$, the instability threshold of the flexible rotor system with the 3-WESB is smaller than that of the rotor system without the 3-WESB in the range of $\sigma = 0.1$ to $\sigma = 0.75$ and again in the range of $\sigma = 0.98$ to $\sigma = 2$. It is however larger than that of the system without the 3-WESB in the range of $\sigma = 0.75$ to $\sigma = 0.98$. The maximum instability threshold occurs at $\sigma = 0.95$ with $a = 9.5$.

Further variation of the value of ζ_3 from 0.02 to 0.09 in Figs. 9 to 12 portrays the same picture as observed in Fig. 8 with the values of the instability thresholds differing. Also the range of σ at which the instability threshold of the rotor system with the 3-WESB is larger than that of the rotor system without the 3-WESB varies with the ζ_3 value. The lower limit of the range of σ decreases $(0.75 \to 0.7 \to 0.65 \to 0.60 \to 0.58)$ whilst the upper limit increases $(0.98 \to 1.05 \to 1.10 \to 1.13 \to 1.15)$ as ζ_3 increases. However, the maximum of the instability threshold increases first and then decreases $(9.5 \to 10.1 \to 10.7 \to 10.3 \to 10.2)$ as ζ_3 increases from 0.01 through to 0.09. $a = 10.7$ is the maximum of the instability threshold at $\sigma = 0.99$ when $\zeta_3 = 0.04$.

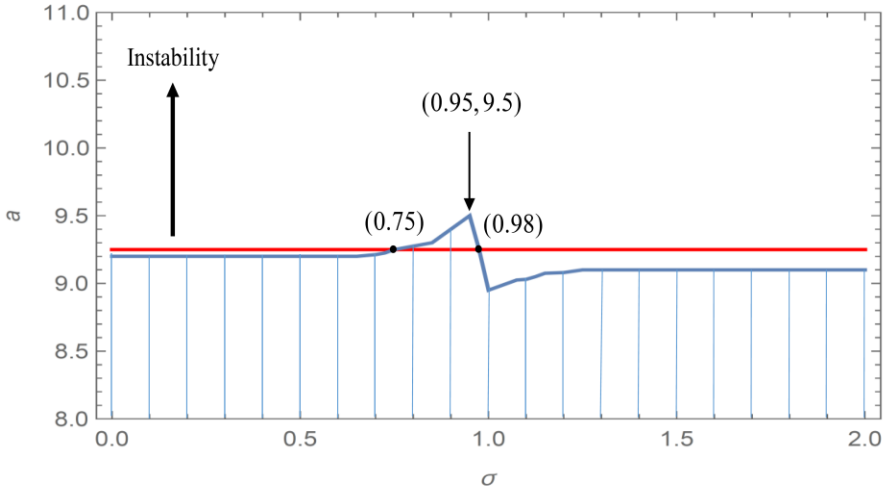

Fig. 8. Stability diagram of the rotor-3-WESB system when $\zeta_3 = 0.01$.

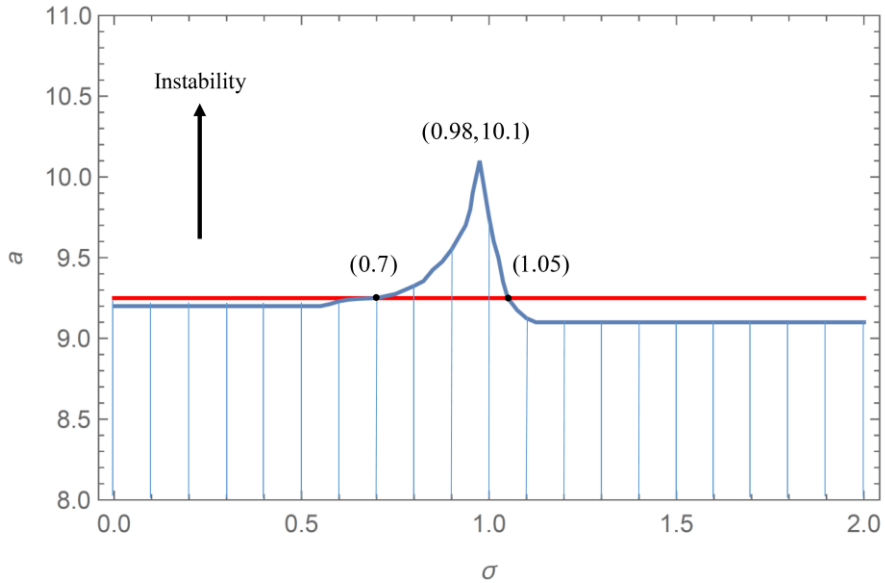

Fig. 9. Stability diagram of the rotor-3-WESB system when $\zeta_3 = 0.02$.

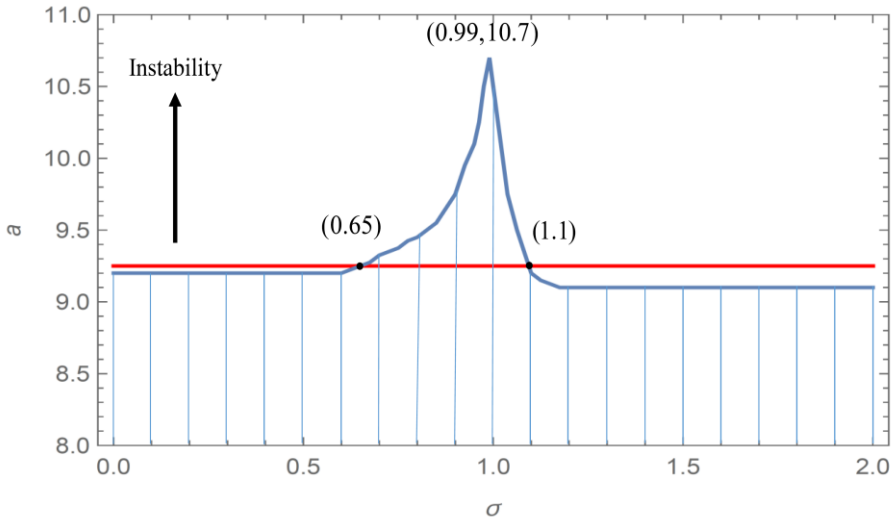

Fig. 10. Stability diagram of the rotor-3-WESB system when $\zeta_3 = 0.04$.

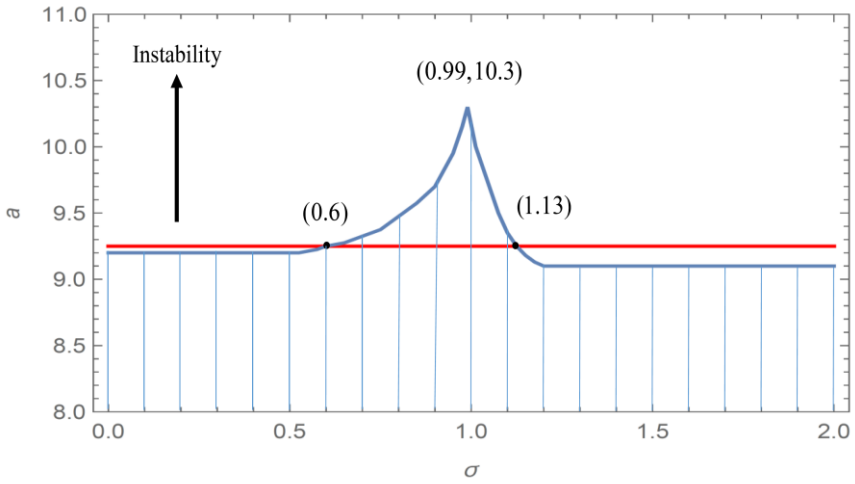

Fig. 11. Stability diagram of the rotor-3-WESB system when $\zeta_3 = 0.07$.

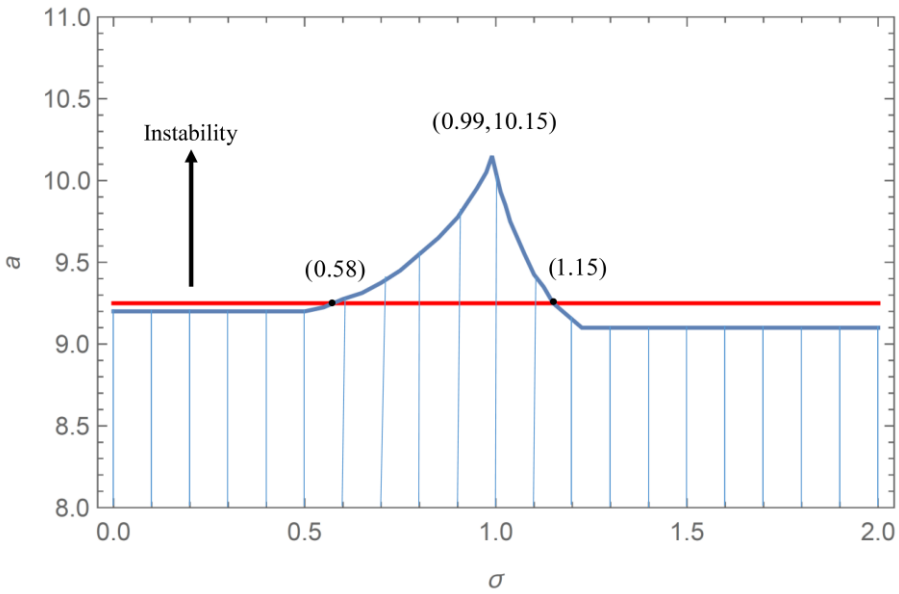

Fig.12. Stability diagram of the rotor-3-WESB system when $\zeta_3 = 0.09$.

VI. CONCLUSION

The present paper has studied the effect of the 3-WESB on the nonlinear dynamic behaviour and stability of the mass unbalanced vibration of the flexible rotor system. The mathematical model of the rotor-3-WESB system is established. The perturbation method of multiple scales is used to solve the differential equations. The effects of the frequency and damping ratios of the 3-WESB on the dynamic behaviour of the mass unbalance induced vibration in the rotor system are discussed. The complex characteristic equation is deduced for the stability analysis and the effects of the 3-WESB on the stability region of the vibration in the rotor system are obtained. Some conclusions are as follows:

1. The frequency response of the amplitude obtained from the multiple scales method agrees with the numerical integration method.
2. Using the 3-WESB with the manipulations of some parameters, the resonant response of the amplitude can be suppressed and the jump phenomena can be effectively eliminated.
3. It has been shown that two design parameters, the stiffness and damping ratios of the 3-WESB have interactive influence of each other on the performance of the flexible rotor system.
4. The instability threshold of the flexible rotor system is changed by the 3-WESB. The instability threshold is decreased by the 3-WESB in some design parameter ranges.

The main contribution of this work is the examination of the first mode response of the nonlinear flexible rotor system using a novel 3-way end-stops bearing. For further research, the author will work on the sub-harmonic and super-harmonic resonant solutions and test the 3-Way end-stop bearing experimentally.

REFERENCES

[1]. Bachschmid N, Pennacchi P and Vania A. Steam-whirl analysis in a high pressure cylinder of a turbo generator. Mech Syst Signal Pr 2008; 22: 121–132.
[2]. Muszynska A. Rotordynamics. Boca Raton, FL: CRC Press, Taylor & Francis Group, 2005.
[3]. Zhang S, Gu Z and Zhang Z. Dynamic balancing method for the single-threaded, fixed-pitch screw rotor.Vacuum 2013; 90: 44–49.
[4]. Atepor, L., (2008). Vibration analysis and control of flexible rotor systems using smart materials. PhD Thesis. University of Glasgow, UK.
[5]. Atepor, L., (2009). Controlling flexible rotor vibration using parametric Excitation. 7th International Conference on Modern Practice in Stress and Vibration Analysis. Journal of Physics: Conference Series 181 (2009) 012021.
[6]. Hemmatian M and Ohadi A. Sliding mode control of flexible rotor based on estimated model of magnetorheological squeeze film damper. J Vib Acoust 2013; 135: 051023.
[7]. Queiroz MD. An active hydrodynamic bearing for controlling self-excited vibrations: theory and simulation. J Vib Control 2012; 19: 2211–2222.
[8]. Janik, T.K and Irretier, H., (1998), New excitation and response measurement techniques for modal testing of flexible rotors. Proceedings of the IFTOMM Conference on Dynamics, Darmstadt, pp.695-708.
[9]. Rade, D.A., Deü, J.-F., Castello, D.A., de Lima, A.M.G. and Rouleau, L., (2019). Passive vibration control using viscoelastic materials. http://www.researchgate.net/publication/331767219. Chapter. January 2019.
[10]. Ribeiro EA, Pereira JT and Alberto Bavastri C. Passive vibration control in rotor dynamics: optimization of composed support using viscoelastic materials. J Sound Vib 2015; 351: 43–56.
[11]. Cartmell, M.P., Ziegler, S.W., Khanin, R. and Forehand, D.I.M., (2003). Multiple scales analysis of the dynamics of weakly nonlinear mechanical systems. Appl Mech Rev 56 (5):255-491.
[12]. Nayfeh, A.H., Mook, D.T., (2004). Nonlinear Oscillations. Wiley-VCH Verlag GmbH & Co. KGaA, Weinheim.

Lawrence Atepor. " Vibration Analysis and Suppression of Flexible Rotor Systems using a 3-Way Viscoelastic Bearing." *American Journal of Engineering Research (AJER)*, vol. 9(8), 2020, pp. 99-109.